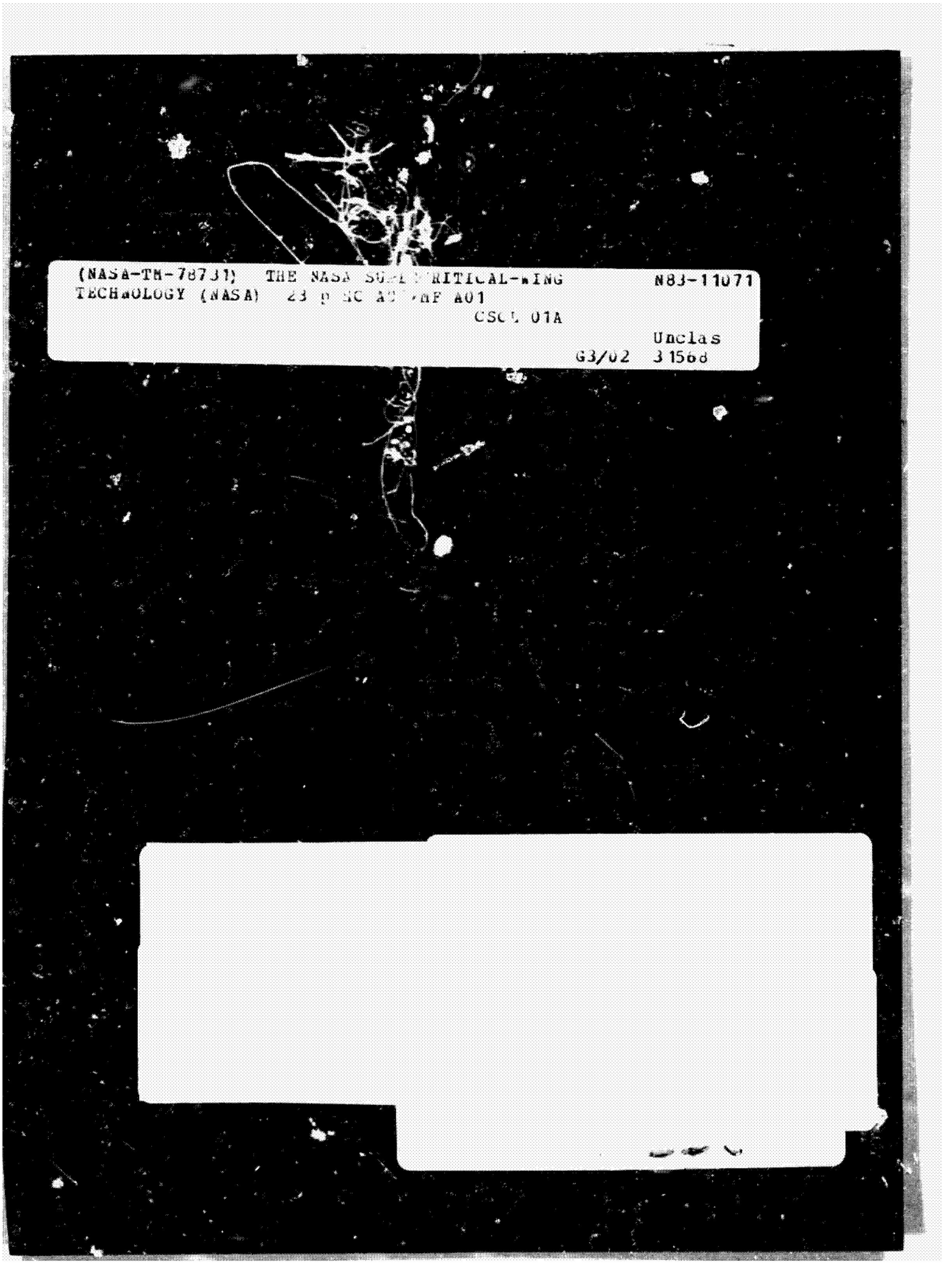

(NASA-TM-78731) THE NASA SUPERCRITICAL-WING TECHNOLOGY (NASA) 23 p HC A02/MF A01
CSCL 01A
N83-11071
Unclas
G3/02 31568

NASA Technical Memorandum 78731

NASA Supercritical-Wing Technology

Dennis W. Bartlett and James C. Patterson, Jr.
Langley Research Center
Hampton, Virginia

National Aeronautics
and Space Administration

**Scientific and Technical
Information Office**

1978

SUMMARY

As part of the Langley Research Center aeronautical research program, a number of high-aspect-ratio supercritical wings in combination with a representative wide-body fuselage have been tested in the Langley 8-foot transonic pressure tunnel. For comparison, data were also obtained on a reference wide-body transport wing tested on the same fuselage. On the basis of these tests, a supercritical wing having an aspect ratio of 9.8, a quarter-chord sweep of 30°, a thickness-to-chord ratio of approximately 0.12 at the mean aerodynamic chord, and a wing design lift coefficient of 0.57 was selected for further study and development. The selected configuration, which was modified to provide increased structural depth at the wing root, has a cruise lift-drag ratio 16 percent higher than a reference wide-body transport configuration and, based on a simplified structural analysis, the selected super-critical wing is approximately equivalent in weight to the wing of the reference wide-body configuration.

As part of a future, extensive wind-tunnel investigation of propulsion/airframe integration, an initial exploratory wind-tunnel test has been conducted to determine the most favorable spanwise nacelle location; pylon airfoil-section shape; and pylon cant angle for a representative twin-engine, supercritical-wing configuration with long-duct, flow-through nacelles. Results from this test indicate a favorable effect of nacelles on the drag-rise Mach number of the configuration at a lift coefficient of 0.60.

INTRODUCTION

As part of the Langley Research Center aeronautical research program and in support of the Energy Efficient Transport element of the NASA Aircraft Energy Efficiency project, a number of high-aspect-ratio supercritical wings in combination with a representative wide-body fuselage have been tested. For comparison, data were also obtained on a reference wide-body transport configuration. The present supercritical wings, relative to existing subsonic transport wings, have higher aspect ratios, greater section thickness-to-chord ratios, and reduced sweepback. Also, as a result of the reduced sweep and higher aspect ratio, the relative areas of such wings would probably be reduced without degrading take-off and landing performance. Compared with earlier NASA supercritical wings (ref. 1), the present wings incorporate refined airfoils (refs. 2 and 3) with reduced drag coefficients at cruise and improved off-design characteristics.

The results of the present paper have been divided into three sections: a systematic investigation of high-aspect-ratio supercritical wings, root-section and planform modifications to a configuration selected from the systematic investigation, and an investigation of interference drag due to long-duct, flow-through nacelles. The wing parameters studied in the systematic investigation include thickness-to-chord ratio, camber, aspect ratio, and sweep. Lift-drag ratios for these configurations are compared with those for the reference wide-body transport configuration, and the effect of the wing section parameters on buffet onset is also presented. To provide increased structural depth at the wing root with no aerodynamic penalties, a larger trailing-edge extension and a leading-edge extension were incorporated in the selected configuration design. Results for this modified configuration are also compared with those for the reference wide-body transport configuration. As part of a future, extensive wind-tunnel investigation of propulsion/airframe integration, an initial exploratory wind-tunnel test has been conducted using long-duct, flow-through nacelles to determine the most favorable spanwise nacelle location; pylon airfoil section shape; and pylon cant angle for a representative twin-engine, supercritical-wing transport configuration. Results are presented that show the effect of the nacelle configurations on the drag-rise characteristics and the wing-section pressure distributions.

The results of the present investigations were obtained from tests conducted in the Langley 8-foot transonic pressure tunnel. A description of this tunnel is contained in reference 4. All tests were conducted at a Reynolds number of 16.4×10^6 per meter (5×10^6 per foot).

SYMBOLS AND ABBREVIATIONS

Values are given in both SI and U.S. Customary Units. The measurements and calculations were made in U.S. Customary Units.

AR	aspect ratio
b	wing span
c	wing streamwise chord
C_D	wing-body drag coefficient
C_L	wing-body lift coefficient
$(c_l)_{DESIGN}$	section design lift coefficient
C_p	pressure coefficient
L/D	lift-drag ratio
M	Mach number

$R_{(L/D)}$	ratio of L/D for the supercritical-wing configurations to L/D for the reference wide-body configuration
x	distance measured from wing leading edge along a streamwise chord
y	spanwise distance measured normal to model plane of symmetry, 0 at fuselage center line
z	vertical distance measured in a plane normal to both x and y
α	angle of attack, deg
$\Lambda_{c/4}$	sweep angle of wing quarter-chord line, deg

Subscripts:

SCW	supercritical wing
WB	wide body

Abbreviations:

EST.	estimated
L.E.	wing leading edge
L.S.	lower surface
SYM.	symmetrical
T.E.	wing trailing edge
U.S.	upper surface

SYSTEMATIC INVESTIGATION OF HIGH-ASPECT-RATIO SUPERCRITICAL WINGS

Configurations

For the present investigation the wings have reference trapezoidal-planform areas of approximately 0.19 m^2 (2 ft^2) and were tested on a common fuselage having a maximum diameter of 14.54 cm (5.74 in.) and a length of 125.88 cm (49.56 in.). All the models were wing-body combinations that were sting mounted through the back of the fuselage as shown in figure 1. A more complete description of the models and test procedures is contained in reference 5.

Supercritical wings.- For the systematic investigation, three supercritical wings which provided variations in wing-section thickness-to-chord ratio and camber (figs. 2 and 3) were tested. A fourth supercritical wing is planned that will provide a variation in wing twist (fig. 4).

For $\Lambda_{c/4} = 27^{\circ}$ and AR = 12, the thicker wing has maximum streamwise thickness-to-chord ratios of 0.16 at the fuselage side, 0.14 at the planform break, and 0.12 at the tip. The thinner supercritical wing has maximum streamwise thickness-to-chord ratios of 0.144, 0.12, and 0.10 at the same stations, respectively (fig. 2). These wings utilize current NASA supercritical airfoils at the planform break and tip stations (refs. 2 and 3); the airfoils have section design lift coefficients of 0.7 and are oriented in a streamwise direction for a quarter-chord sweep angle of 27°. The airfoil at the wing-fuselage juncture is not a typical supercritical airfoil, and it will be discussed in a subsequent section. Coordinates for these wings are contained in reference 5. The third supercritical wing tested has the same thickness ratios as the thinner wing described above; however, the camber for the sections on the outer panel is reduced (fig. 3). This reduction in camber corresponds to a decrease in the section design lift coefficient from 0.7 to 0.6. The root airfoil is the same for both wings. The spanwise twist distribution is presented in figure 4. Also shown in figure 4 is the twist distribution for a projected supercritical wing that will have about 2.5° more washout than the wings already tested.

Each supercritical wing was tested at quarter-chord sweep angles of 27° and 30° (fig. 5), and an aspect-ratio variation from 12.0 to 10.3 (based on a trapezoidal planform) was produced by clipping the tips of the thinner wing (fig. 5).

Wide body.- The spanwise thickness-to-chord ratio distribution for the wide-body transport wing varies from 0.123 at the fuselage side to about 0.09 over the outer panel (fig. 2). This wing has about 6.5° of washout, whereas the supercritical wings have 4° of washout (fig. 4). The planform has 35° of sweep at the quarter-chord line and an aspect ratio of 7 (fig. 5), and the wing design lift coefficient is 0.45. Coordinates for this wing are contained in reference 5.

Results

Results from the systematic investigation are presented in figures 6 to 10. The relative lift-drag ratio (presented in figs. 6 to 9) is defined as the ratio of L/D for the supercritical wing configurations at a lift coefficient of 0.60 to L/D for the wide-body configuration at a lift coefficient of 0.45. These lift coefficients are near the maximum L/D for each configuration.

Thickness and camber.- The thickness effect (fig. 6) is presented for the higher cambered wing at $\Lambda_{c/4} = 30^{\circ}$, and the camber effect (fig. 7) is presented for the thinner wing at 27°. As would be expected, R(L/D) for the thicker wing starts to decrease at a lower Mach number and falls off much more abruptly at the higher Mach numbers than R(L/D) for the thinner wing (fig. 6). The lower cambered wing exhibits lower values of R(L/D) throughout

the Mach number range presented than the higher cambered wing (fig. 7). However, it should be mentioned that at a lift coefficient of 0.53, the values of L/D for the two differently cambered wings are practically equal.

Sweep and aspect ratio.- Both the sweep and aspect-ratio effects (figs. 8 and 9, respectively) are presented for the thinner, higher cambered supercritical wing. The 30° swept-wing configuration has higher $R(L/D)$ than the 27° swept-wing configuration at Mach numbers above 0.80. At Mach numbers below 0.80, the lower $R(L/D)$ values for the 30° swept-wing configuration are due to the slightly smaller aspect ratio which results when the wing is swept from 27° to 30° (fig. 8). As might be expected, the configuration with AR = 10.3 has lower $R(L/D)$ values throughout the Mach number range presented (fig. 9) than those for the configuration with AR = 12. At lower lift coefficients, however, the difference would not be as large.

Buffet.- The effect of thickness ratio and camber on buffet onset at a Mach number of 0.80 is presented in the results of figure 10. The first break in the lift curve is being used as an indication of buffet onset and this technique for determining buffet onset is usually conservative. The thicker wing is presented at the 30° sweep angle to give it approximately the same drag-rise Mach number as the two other wings. As seen in figure 10, the thinner, higher cambered supercritical wing has a higher buffet-onset lift coefficient than either the thicker wing of the same camber or the lower cambered wing of the same thickness. (Solid circles indicate buffet onset for each configuration.)

Selected configuration.- Of the configurations tested, the thinner, higher cambered wing (AR = 12, $\Lambda_c/4$ = 27°) provided the highest values of $R(L/D)$. For example, at a Mach number of 0.79 and a lift coefficient of 0.60, this configuration has a value of L/D approximately 31 percent higher than L/D for the wide-body configuration at its design lift coefficient of 0.45. However, in selecting a configuration for further development, several aerodynamic and structural considerations were involved. Therefore, the thinner, higher cambered supercritical wing with 30° of sweep was chosen to provide the highest cruise Mach number with the best buffet margin. In addition, an aspect ratio of 9.8 was selected to avoid any structural and landing-gear installation problems that might occur with an aspect-ratio-12 wing if current construction techniques and materials are assumed. It should be mentioned that the selected configuration with the reduced aspect ratio of 9.8 is intended to have winglets. Data for this configuration with winglets is contained in reference 6.

ROOT-SECTION AND PLANFORM MODIFICATIONS TO THE SELECTED SUPERCRITICAL WING

Modifications

The root-section and planform modifications to the selected supercritical wing are presented in figure 11. The inboard sections shown in figure 11 are located approximately 1.0 cm (0.4 in.) from the fuselage side. The root

section differs from the conventional supercritical airfoils on the outer panel in that it has less aft camber and significantly reduced upper-surface curvature. In addition, the chordwise location of maximum thickness is much farther forward.

The larger trailing-edge extension allowed for a substantial increase in the thickness of the wing root in the region where the rear spar and landing-gear attachment would be located. (See fig. 11.) With the larger trailing-edge extension, the wing inboard trailing-edge sweep angle is 0°. A leading-edge extension was also added to the selected configuration and it increased the inboard leading-edge sweep angle from about 31.8° to 37.3°. (See fig. 11.) The coordinates presented in reference 5 do not include the larger trailing-edge extension or the leading-edge extension.

Results

The effect of these inboard modifications (fig. 11) on the drag-rise characteristics is presented in figure 12 for a lift coefficient of 0.57. (This lift coefficient is more nearly optimum for AR = 9.8.) In adding the larger trailing-edge extension, no performance penalty was incurred; moreover, the leading-edge extension provided an increase in drag-rise Mach number of almost 0.01, with only a small drag penalty at the lower Mach numbers.

The relative lift-drag ratios for the current NASA supercritical-wing configuration (selected configuration with inboard modifications) are presented in figure 13. At a Mach number of 0.80 this configuration has a value of L/D almost 16 percent higher ($R_{(L/D)}$ = 1.16) than L/D for the reference wide-body configuration. Although the higher aspect-ratio, supercritical wings have higher values of L/D than the current configuration, they would also have higher structural weight than the wing of the reference wide-body configuration. However, a simplified structural analysis indicates that the current supercritical-wing configuration with the reduced aspect ratio and increased structural depth at the wing root would be approximately equivalent in weight to that of the wing of the reference wide-body configuration. Furthermore, the optimum wing loading is expected to be higher for aircraft with the present supercritical wing than for current aircraft, not only because of the higher design lift coefficient for cruise, but also because of the expected gain in take-off and landing performance achievable with the higher aspect ratio and lower sweep angle. The corresponding reductions in wing size would result directly in lower wing weight.

A comparison of the buffet onset for the current NASA supercritical-wing configuration and the reference wide-body configuration is provided in the results of figure 14. As in figure 10, the first break in the lift curve is being used as an indication of buffet onset. The solid circles indicate buffet onset for each configuration. Even though the supercritical-wing configuration has a higher cruise lift coefficient, its relative buffet margin is larger than that for the reference wide-body configuration. The higher Mach number presented for the reference wide-body configuration is not a penalty, since the drag-rise Mach number is about 0.1 higher than that for the supercritical-wing configuration.

Recent tests have shown that the thickness on the outer panel can be increased approximately 10 percent at the 80-percent-chord location with no drag penalty. All the extra thickness was added on the lower surface and extended from the planform break to the tip. Although there is no drag penalty associated with this added thickness to the lower surface, there is a reduction in lift coefficient of about 0.01, which affects the buffet onset. (See fig. 15.) Additional increases in thickness to this area of the lower surface would, of course, decamber the wing even further. This additional lower-surface thickness is also not reflected in the coordinates contained in reference 5.

EXPLORATORY INVESTIGATION OF SUPERCRITICAL-WING—PYLON—NACELLE INTERFERENCE USING LONG-DUCT, FLOW-THROUGH NACELLES

Configurations

The representative twin-engine supercritical-wing configuration used for the flow-through nacelle investigation is shown in figure 16. The supercritical wing has an aspect ratio of 10.3, a quarter-chord sweep of 27°, and approximately the same spanwise thickness-to-chord ratio distribution as the thinner supercritical wing of figure 2.

The long-duct, flow-through nacelles were pylon mounted beneath the supercritical wing. Nacelle locations of 30, 43, and 55 percent of the semispan were investigated, and the nacelles were tested with both symmetrical and cambered pylons. The effect of pylon cant angle was also measured. A planform sketch of the model showing the various nacelle locations and a streamwise airfoil section from both the symmetrical and cambered pylon are presented in figure 17. The cambered pylon was obtained by flattening the inboard side of the symmetrical pylon. Also, positive pylon cant angle is an outward movement (toward the wing tip) of the pylon leading edge.

Results

Results of the present investigation indicate that the 43-percent-semispan nacelle location with a cambered pylon having 2° of cant angle is the optimum combination of the parameters tested. Although the most inboard nacelle location (30 percent semispan) results in a higher installation drag than the 43-percent location, its installation drag is less than that of the most outboard location tested (55 percent semispan).

The drag-rise characteristics for the best nacelle-pylon arrangement (43-percent-semispan location with a cambered pylon at +2° cant angle) and a reference nacelle-pylon arrangement (30-percent-semispan location with a symmetrical pylon at 0° cant angle) are presented in figure 18 for a lift coefficient of 0.60. Also presented are the drag-rise characteristics for the basic wing-body (nacelle-off) configuration. The nacelle configuration with the cambered and canted pylon has lower drag throughout the Mach number range than the reference nacelle arrangement. In addition, by superimposing the nacelle-on data on the nacelle-off data (eliminating the difference

in drag coefficient due to skin friction and form drag), it is possible to determine the effect of the nacelle installation on drag-rise Mach number. The results for the symmetrical-pylon configuration are the same as for the nacelles-off configuration; however, the cambered-pylon configuration provides an increase in drag-rise Mach number.

The reason for this favorable effect on drag-rise Mach number can be seen in the streamwise wing-pressure distribution (just inboard of the pylon at the 43-percent-semispan nacelle location) presented in figure 19. On the wing lower surface a shock wave occurs at approximately the 12-percent-chord location with the symmetrical-pylon-nacelle installation. By cambering and canting the pylon, the shock wave is eliminated, and this accounts for the different drag levels between the two nacelle configurations. In addition, both nacelle configurations reduce the strength of the upper-surface shock wave and move it forward. The forward movement of the shock wave is an indication of a reduction in the effective local Mach number for this wing station, and this results in the favorable effect of the nacelles on the drag-rise Mach number.

The most favorable spanwise nacelle location, pylon airfoil shape, and pylon cant angle determined during these tests are being incorporated in the design of a semispan model which will use powered nacelles to determine the effect of the jet wake on the interference drag (ref. 7).

SUMMARY OF RESULTS

A systematic wind-tunnel investigation has been conducted on high-aspect-ratio supercritical wings in combination with a wide-body fuselage. In addition, an exploratory investigation has been conducted of supercritical-wing—pylon—nacelle interference using long-duct, flow-through nacelles. The following results were obtained:

1. A configuration having an aspect ratio of 9.8, a quarter-chord sweep of 30°, a thickness-to-chord ratio of approximately 0.12 at the mean aerodynamic chord, and a wing design lift coefficient of 0.57 was selected for further development.

2. The selected configuration, which was modified near the root to provide increased structural depth, has a cruise lift-drag ratio 16 percent higher than a reference wide-body configuration. Based on a simplified structural analysis, the relative weights of the two wings would be approximately the same.

3. An exploratory wind-tunnel investigation of long-duct, flow-through nacelles with properly designed pylons indicates a favorable effect of nacelles on the drag-rise Mach number of a supercritical-wing configuration at a lift coefficient of 0.60.

Langley Research Center
National Aeronautics and Space Administration
Hampton, VA 23665
June 7, 1978

REFERENCES

1. Supercritical Wing Technology - A Progress Report on Flight Evaluations. NASA SP-301, 1972.

2. Harris, Charles D.: Aerodynamic Characteristics of the 10-Percent-Thick NASA Supercritical Airfoil 33 Designed for a Normal-Force Coefficient of 0.7. NASA TM X-72711, 1975.

3. Harris, Charles D.: Aerodynamic Characteristics of a 14-Percent-Thick NASA Supercritical Airfoil Designed for a Normal-Force Coefficient of 0.7. NASA TM X-72712, 1975.

4. Schaefer, William T., Jr.: Characteristics of Major Active Wind Tunnels at the Langley Research Center. NASA TM X-1130, 1965.

5. Bartlett, Dennis W.: Wind-Tunnel Investigation of Several High Aspect-Ratio Supercritical Wing Configurations on a Wide-Body-Type Fuselage. NASA TM X-71996, 1977.

6. Flechner, Stuart G.; and Jacobs, Peter F.: Experimental Results of Winglets on First, Second, and Third Generation Jet Transports. CTOL Transport Technology - 1978, NASA CP-2036, Pt. II, 1978, pp. 553-569. (Also available as NASA TM-72674.)

7. Patterson, James C., Jr.: A Wind-Tunnel Investigation of the Jet-Wake Effect of a High-Bypass Engine on Wing-Nacelle Interference Drag of a Subsonic Transport. NASA TN D-4693, 1968.

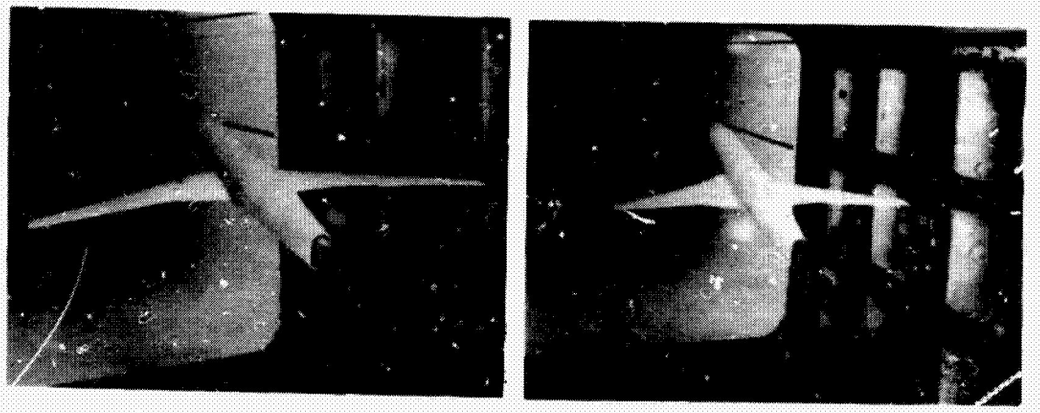

SUPERCRITICAL WING
ASPECT RATIO = 12.0

REFERENCE WIDE BODY
ASPECT RATIO = 7.0

Figure 1.- Wind-tunnel models.

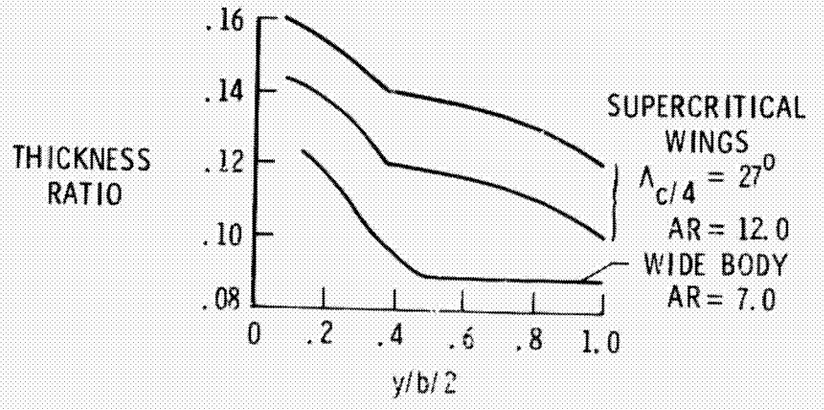

Figure 2.- Spanwise thickness-to-chord ratio distributions

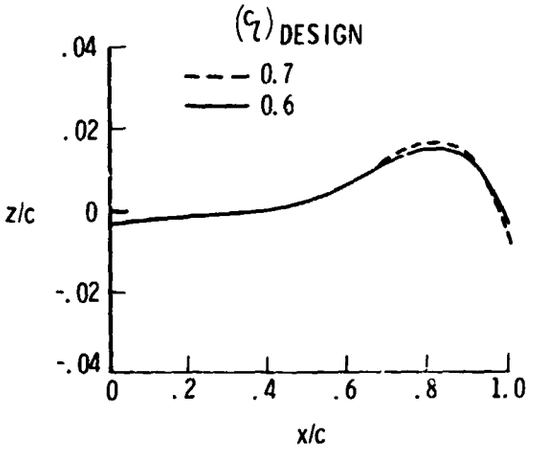

Figure 3.- ι-line coordinates for the mean geometric chord (thinner wing).

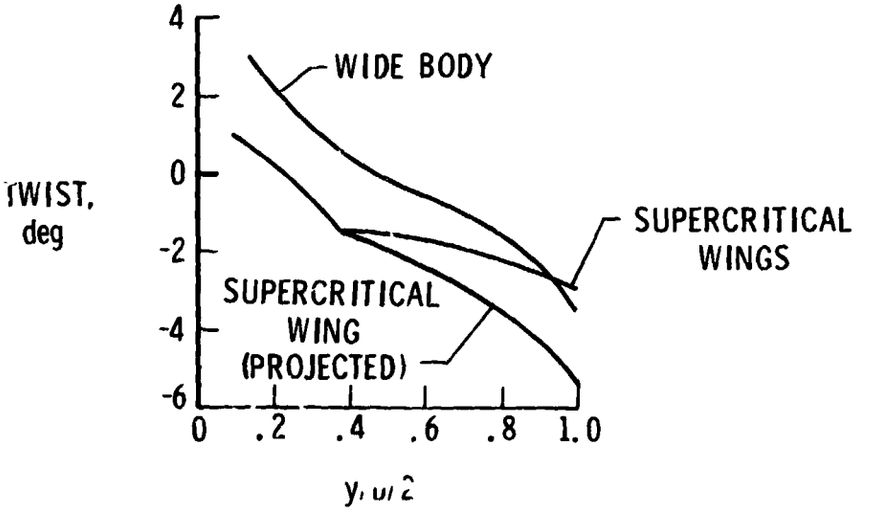

Figure 4.- Spanwise twist distributions.

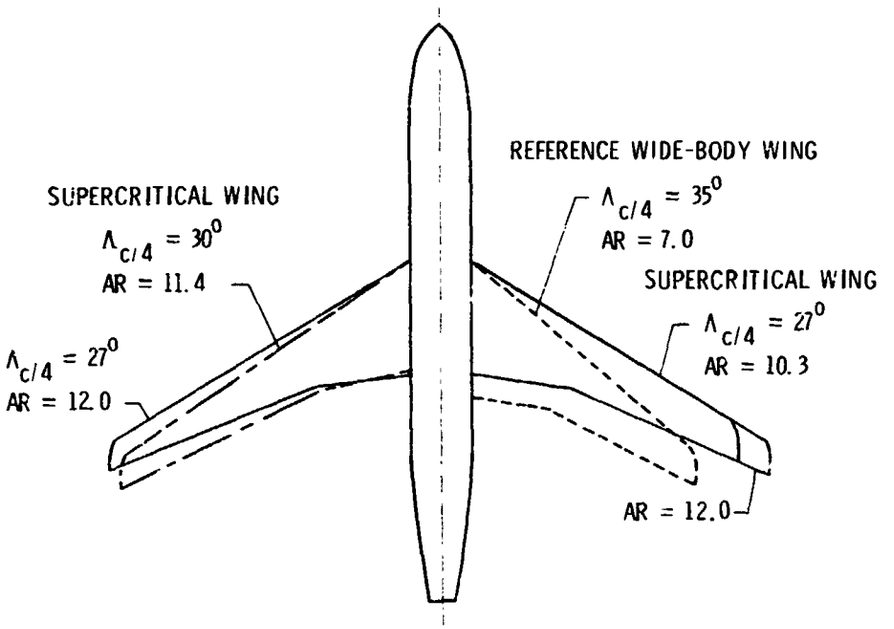

Figure 5.- Planform variables.

$$\left\{ R_{(L/D)} = \frac{(L/D)_{SCW}}{(L/D)_{WB}} \quad \begin{matrix} @\ C_L = 0.60 \\ @\ C_L = 0.45 \end{matrix} \right\}$$

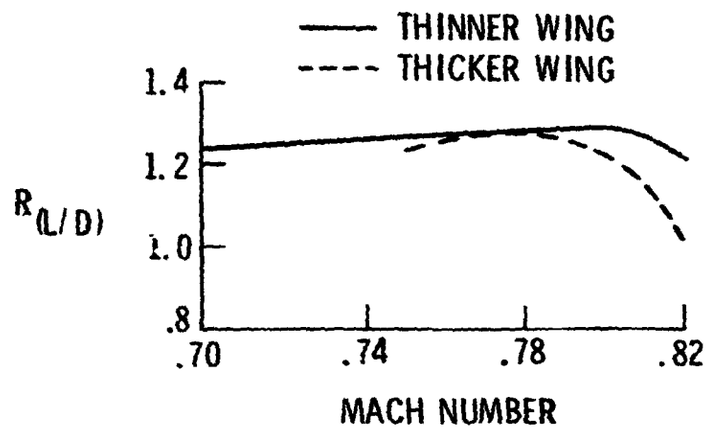

Figure 6.- Effect of section thickness on $R_{(L/D)}$. $(c_l)_{DESIGN} = 0.7$; $\Lambda_{c/4} = 30^{\circ}$; AR = 11.4.

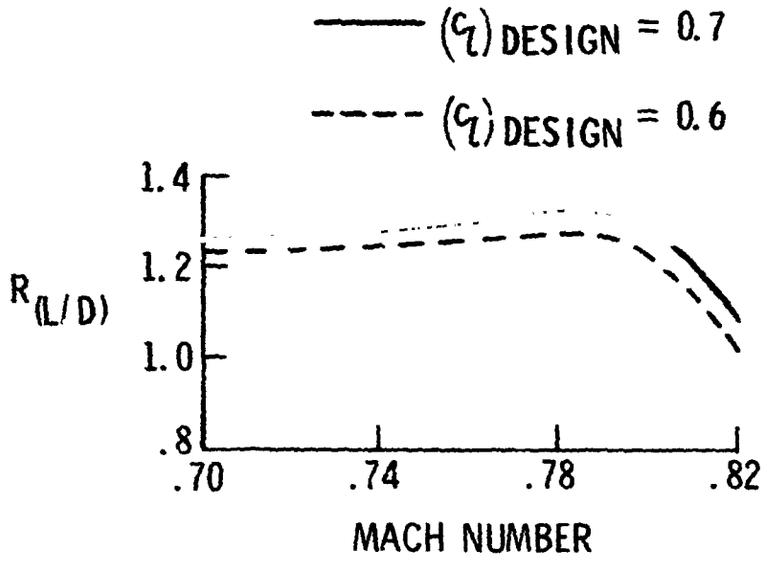

Figure 7.- Effect of section camber on $R_{(L/D)}$. Thinner wing; $\Lambda_{c/4} = 27^{\circ}$; AR = 12.0.

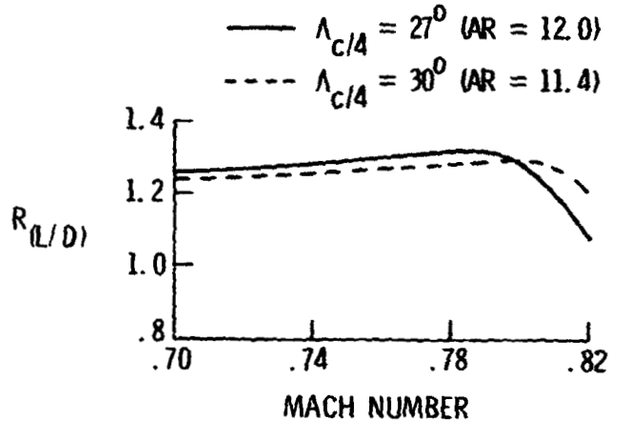

Figure 8.- Effect of wing sweep on $R_{(L/D)}$. Thinner wing; $\left(c_l\right)_{DESIGN} = 0.7$.

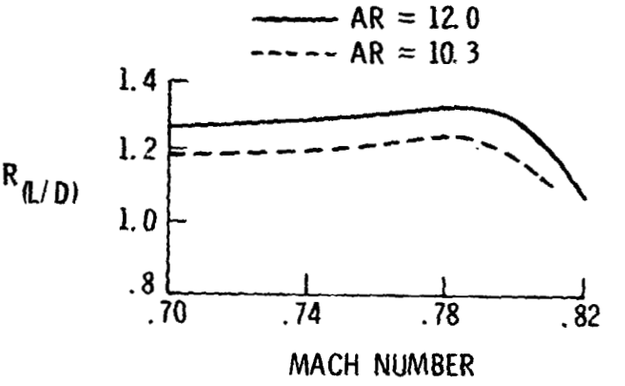

Figure 9.- Effect of aspect ratio on $R_{(L/D)}$. Thinner wing; $\left(c_l\right)_{DESIGN} = 0.7$; $\Lambda_{c/4} = 27^{o}$.

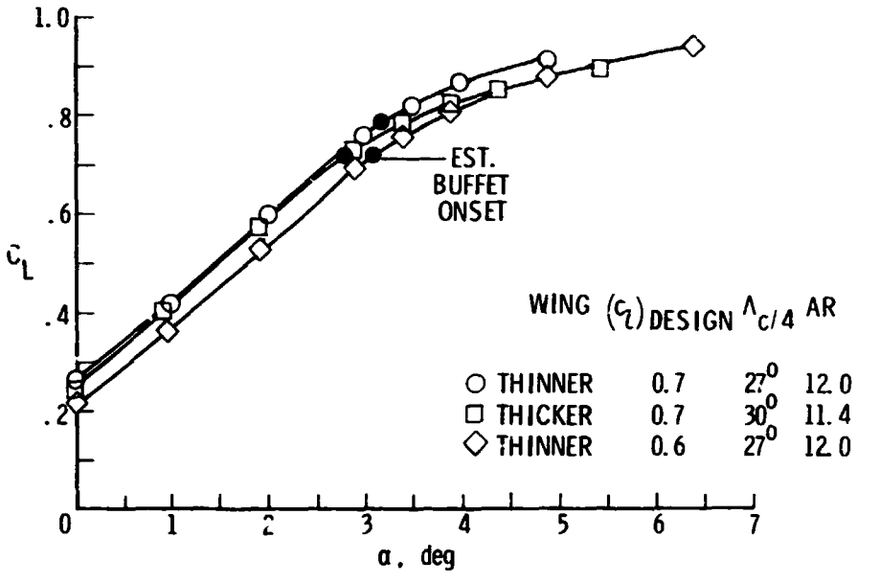

Figure 10.- Effect of section varibles on buffet onset at M = 0.80.

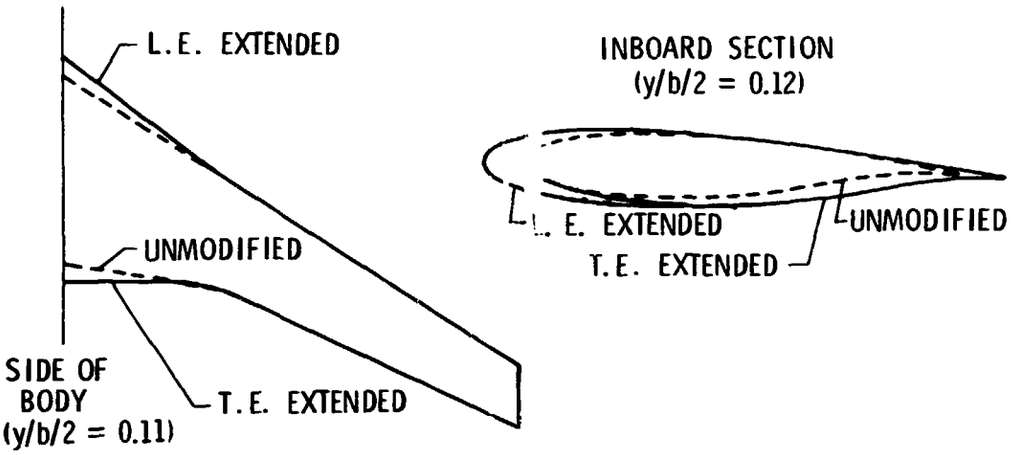

Figure 11.- Root-section and planform modifications to the selected supercritical wing. $\Lambda_{c/4}$ = 30°; AR = 9.8.

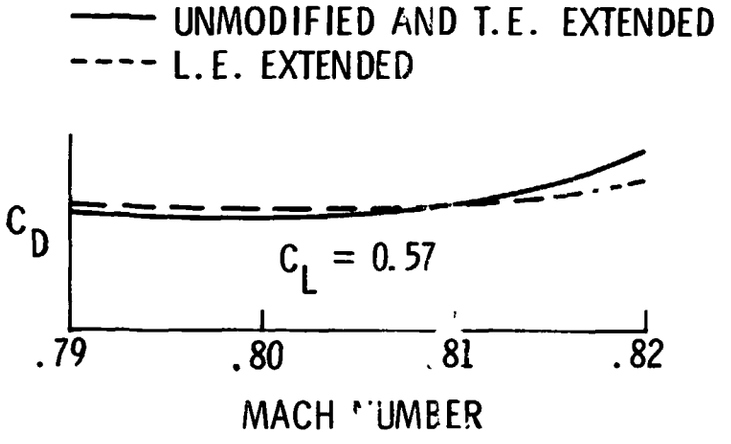

Figure 12.- Effect of root section and planform modifications on drag-rise characteristics.

$$\left\{ R_{(L/D)} = \frac{(L/D)_{SCW}}{(L/D)_{WB}} \quad \begin{matrix} @\ C_L = 0.57 \\ @\ C_L = 0.45 \end{matrix} \right\}$$

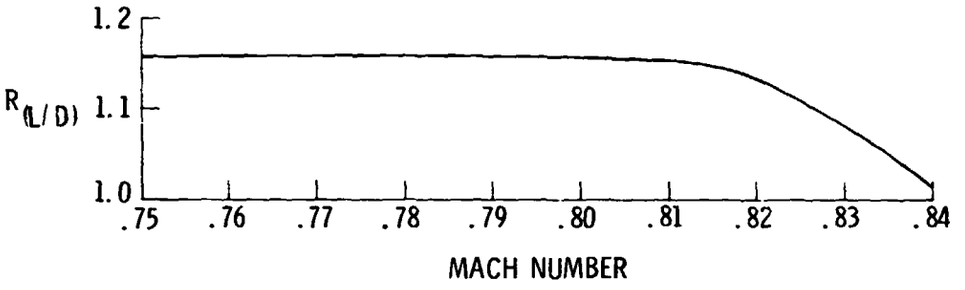

Figure 13.- Relative lift-drag ratio for the current NASA configuration.

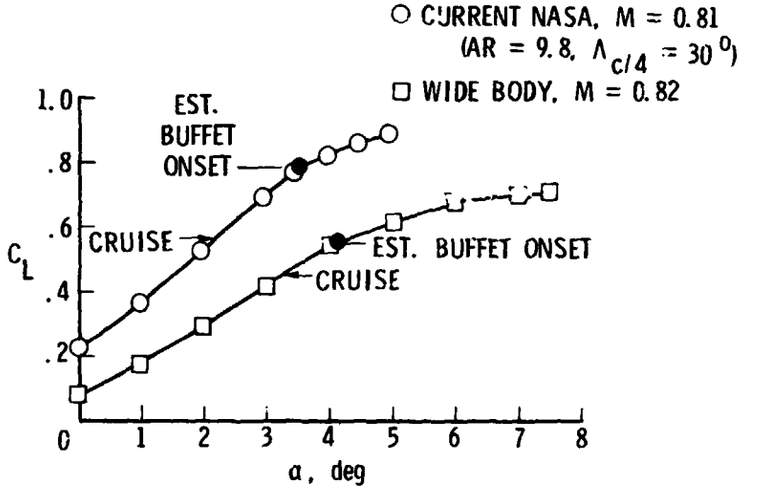

Figure 14.- Comparison of buffet onset for the current NASA and the reference wide-body configurations.

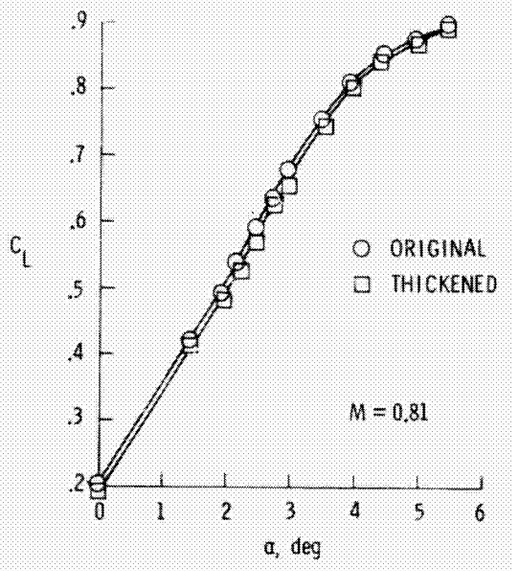

Figure 15.- Experimental effect of thickening supercritical wing outer panel at 80 percent chord.

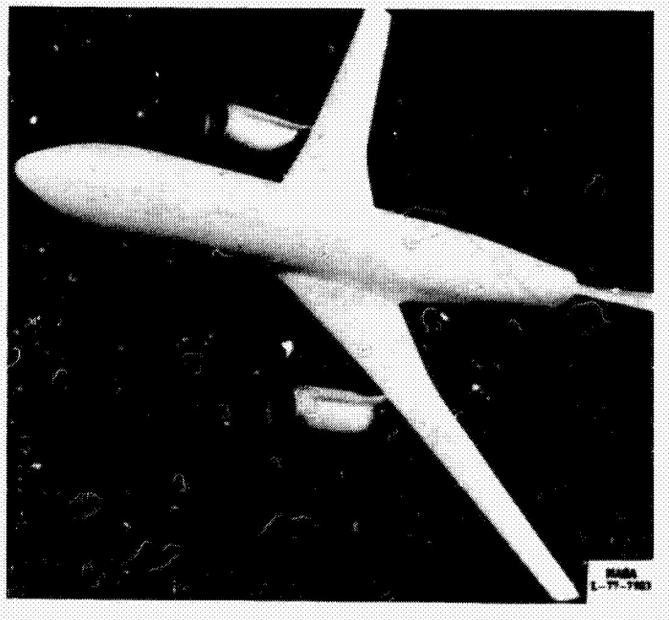

Figure 16.- Wind-tunnel model with long-duct, flow-through nacelles.

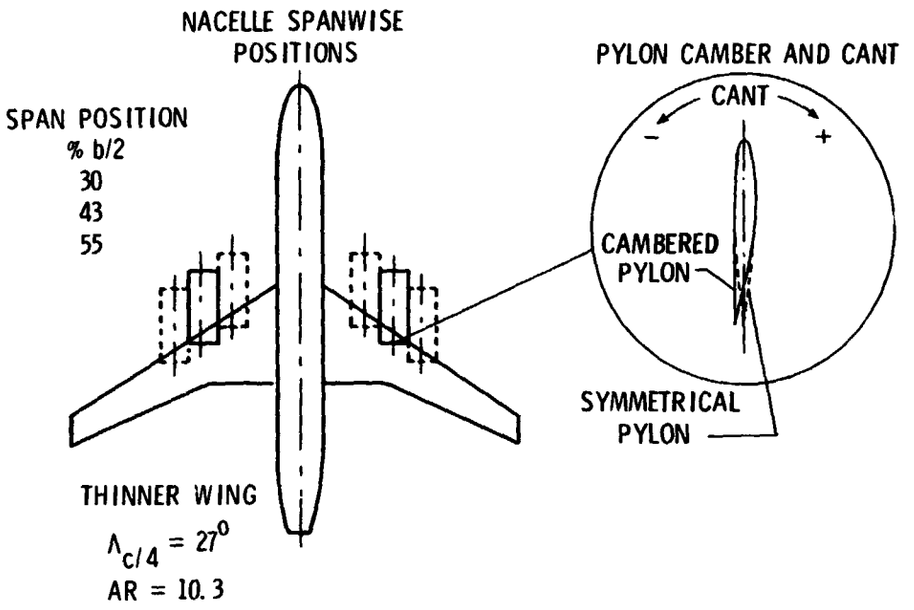

Figure 17.- Flow-through nacelle configurations.

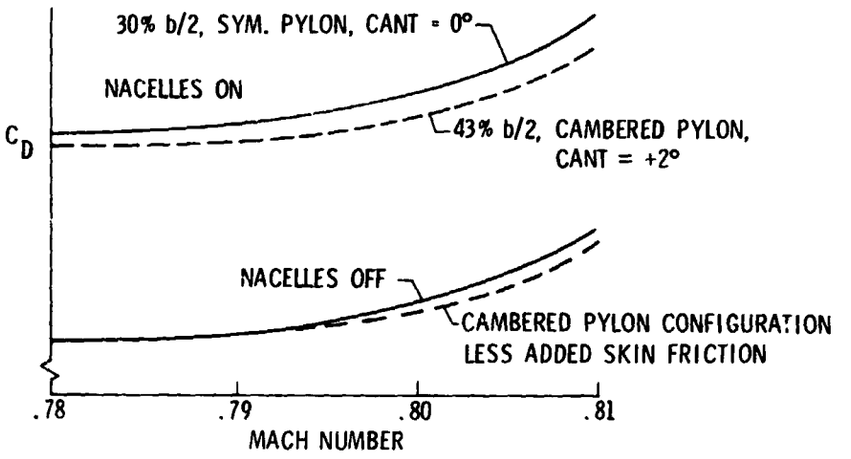

Figure 18.- Effect of nacelles on drag-rise characteristics at $C_L = 0.60$. $\Lambda_{c/4} = 27^0$; AR = 10.3.

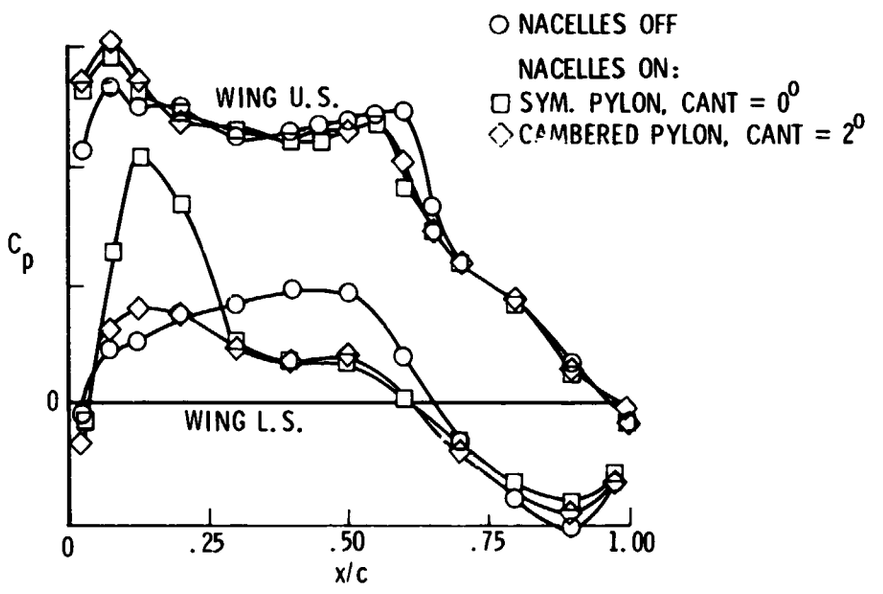

Figure 19.- Effect of nacelles on wing pressure distribution (inboard of pylon at 43 percent b/2).